Biophysical Chemistry 41 (1991) 143–156
Elsevier Science Publishers B.V., Amsterdam

BIOCHE 01585

Electrical characteristics in an excitable element of lipid membrane

Kiyoshi Toko [a,*], Norimasa Ozaki [a], Satoru Iiyama [b], Kaoru Yamafuji [a], Yoshiko Matsui [c], Keiko Yamafuji [c], Minoru Saito [d] and Masakazu Kato [d]

[a] *Department of Electronics, Faculty of Engineering, Kyushu University 36, Fukuoka 812 (Japan)*
[b] *Department of Home Economics, Kyushu Junior College of Kinki University, Iizuka 820 (Japan)*
[c] *Department of Food and Nutrition, Nakamura Gakuen College, Fukuoka 814 (Japan), and*
[d] *Oki Electric Industry Co., Ltd., Hachioji, Tokyo 193 (Japan)*

(Received 24 May 1990; accepted in revised form 5 March 1991)

Abstract

Electrical characteristics in a membrane constructed from a porous filter adsorbed with a lipid analogue, dioleyl phosphate (DOPH), were investigated in a situation interposed between 100 m*M* NaCl + 3 m*M* $CaCl_2$ and 100 m*M* KCl. Calcium ions affected significantly the membrane characteristics. The membrane potential was negative on the KCl side, which implies the higher permeability to K^+ than Na^+; this tendency was increased by a tiny amount of Ca^{2+}. While the membrane showed a low electrical resistance of several $k\Omega \cdot cm^2$ under K^+/Na^+ gradient, it showed several $M\Omega \cdot cm^2$ by Ca^{2+}. The surface structure of the membrane exhibited many voids in the low-resistance state, but the surface was covered by oil droplets in the high-resistance state. Oscillations of the membrane potential appeared spontaneously with application of the electrical current from the KCl side to the NaCl + $CaCl_2$ side. The frequency was increased with the electrical current. All these results were explained comprehensively using an electrochemical kinetic model taking account of the Ca^{2+} binding effect, where DOPH assemblies make a phase transition between oil droplets due to Ca^{2+} and multi-bilayers with excess K^+. The oscillation arises from coupling of the phase transition to accumulation and release of K^+ or Ca^{2+}. This membrane can be used as an excitable element regulated by Ca^{2+} in neuro-computer devices.

Keywords: Lipid membrane; Phase transition; Oscillation; Excitability; Ca^{2+} binding; Neuro-computer

1. Introduction

A DOPH-adsorbed porous membrane is composed of a Millipore filter, the pores of which are choked up with a lipid analogue, dioleyl phosphate (DOPH). This membrane shows a self-sustained oscillation of the membrane potential under a d.c. electrical current and pressure difference across the membrane depending on the concentration gradient or a salt such as KCl [1–6]. This phenomenon is attributed to a repeated phase transition of DOPH assembly formed in pores, where the transition occurs at some critical concentration of the salt ($\simeq$ 30 m*M*) between hydrophobic oil droplets at lower salt concentrations and hydrophilic micelles or bilayer (or multilayer) leaflets at higher concentrations [7,8].

* To whom correspondence should be addressed.

Biological systems contain mainly K^+ ions inside the cell, and outside mainly Na^+ ions and low concentration of Ca^{2+} ions, which are adsorbed to the surface of the cell membranes to maintain the membrane potential and resistance at resting levels [9]. Electrical or chemical stimuli elicit a transient change in the membrane potential or repetitive firing, i.e., excitation. Development of an artificial nerve membrane may require a study of excitable model membranes under experimental conditions close to the biological system. These kinds of Ca^{2+}-regulated artificial nerve membranes can be useful for elements in neurocomputer devices, which have been recently studied vigorously from the viewpoint of software [10].

No experiments, however, where conditions are essentially the same as in the biological situation have been performed so far. For example, experiments were made by placing the DOPH membrane between 100 m*M* KCl and 5 m*M* KCl solutions [1–5]. Oscillations were reported for the same membrane under the 100 m*M* Na^+/100 m*M* K^+ gradient [6] and 100 m*M* K^+/100 m*M* K^+ with approximately 1 m*M* Ca^{2+} [11–13]. Oscillatory behaviors in other types of artificial membranes were also studied in a concentration gradient of ions between K^+ and Na^+ [14].

In the present paper, we study a mechanism of oscillations under 100 mM Na^+/100 m*M* K^+ gradient with Ca^{2+}. Although previous work [11–13] showed an important role of Ca^{2+} on the excitability of lipid membranes, no theoretical analysis has been made so far. It seems, therefore, better for the detailed theoretical comparison to perform systematic experiments on the static and dynamic properties of the DOPH membrane under Na^+, Ca^{2+}/K^+ gradient. In addition, we observed the surface structure of the membrane in relation to the membrane resistance, because the aggregation state of DOPH molecules may be essential in the electrical change in the membrane. Whereas the membrane resistance may be supposed to decrease in the excitation in oscillations [4,5,11,12], it is necessary to measure directly the change in membrane resistance during the oscillation; hence we measured it by superimposing the sine wave on the d.c. current applied on the membrane. The membrane potential under Na^+, Ca^{2+}/K^+ gradient was also measured to study effect of each ion on the membrane.

All these experimental results were explained based on a theoretical model constructed from three equations for the state of DOPH assemblies and the ion concentrations. The mechanism of the oscillation was discussed from the point of view that Ca^{2+} ions affect a phase transition of DOPH molecules in the pores.

2. Materials and methods

The DOPH-adsorbed membranes were prepared by the same method as reported previously [3–5]. The amount of DOPH adsorbed on a filter paper (average pore size ~ 5 μm) was adjusted to about 3.5 mg/cm^2. Whereas the membranes were immersed in 100 m*M* KCl solution and then in 1 m*M* KCl solution before measurements in the previous work [6], they were immersed in only 100 m*M* KCl solution over 12 hours in the present work to make the membrane resistance as low as several kΩ. As shown in Fig. 1, each membrane was interposed between two cells with two pairs of Ag–AgCl electrodes, one of which was used for the measurement of membrane potential or voltage difference across the membrane, the other

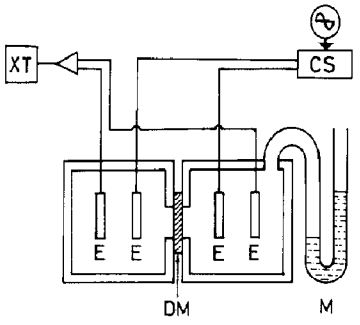

Fig. 1. Schematic of experimental apparatus. A DOPH-Millipore membrane (DM) was placed between two cells, each containing an $NaCl+CaCl_2$ or a KCl solution. An area of about 1 cm^2 of the membrane was exposed to the solutions. The membrane potential was detected with Ag–AgCl electrodes (E) and recorded on a pen-type X-T recorder (XT). The pressure and electrical current were applied by means of a manometer (M) and an oscillator-controlled current source (CS), respectively.

being for the current supply. One cell contained a 100 mM KCl solution and the other a 100 mM NaCl solution. $CaCl_2$ was added to the cell which contained NaCl.

The membrane potential was recorded on an X–T recorder (XT) by grounding one electrode in the cell occupied by the NaCl solution. When the d.c. electrical current and the pressure were necessary for occurrence of electrical oscillations, they were applied using a current source (CS) and a manometer (M), respectively.

The membrane resistance R_m when the oscillation occurs was measured by superimposing the sine wave on the d.c. component using the oscillator-controlled current supply. The resistance can be evaluated from the amplitude.

The surface structure of the membrane was observed by use of a scanning electron microscope (SEM). The membranes were desiccated overnight with silica gel beads and sputtered with gold ions at 1 kV × 5 mA for 25 minutes by an ion sputter (JEOL F-1100). These gold-sputtered membranes were scanned at ~ 10–15 kV and photographed by a JOEL JSM-T300 SEM apparatus.

3. Experimental results

3.1 Effect of Ca^{2+} on membrane resistance

The membrane resistance showed low values when the membrane was placed between 100 mM KCl and 100 mM NaCl, as shown in Fig. 2. Addition of $CaCl_2$ to the 100 mM NaCl solution suddenly increased the resistance to several MΩ above a critical concentration, in agreement with the previous report [11]. The solid line in Fig. 2 was theoretically obtained.

When the membrane was placed between 100 mM KCl and 100 mM NaCl, the membrane potential showed a negative value as small as approximately −10 mV (Fig. 3), which implies that the membrane is a little more permeable to K^+ than Na^+. While the membrane resistance became higher with addition of approx. 1 mM $CaCl_2$, the membrane potential was still negative and further decreased. At the higher $CaCl_2$ concentration of approx. 5 mM, however, the membrane potential became positive.

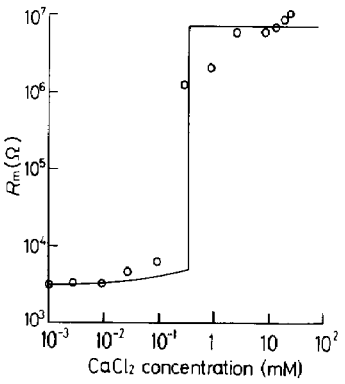

Fig. 2. Increase in the membrane resistance, R_m, caused by addition of Ca^{2+}. Experimental data are denoted by circles (○) and the theoretical curve of eqs. (4) and (5) is shown by a solid line (—). The parameter values are summarized in Table 1. A membrane was placed between 100 mM KCl and 100 mM NaCl solution, to which $CaCl_2$ was added. The resistance without $CaCl_2$ was the same as that with 10^{-3} mM $CaCl_2$.

3.2 Effect of KCl on $[Ca]_c$

Figure 4 shows the dependence of the critical Ca^{2+} concentration to cause the high resistance, $[Ca]_c$, on the KCl concentration, the theoretical curve being shown by a solid line. The KCl concentration in one cell was increased with 100 mM NaCl and an arbitrary $CaCl_2$ concentration included in the other cell. Further increasing the KCl concentration resulted in an abrupt decrease of the membrane resistance. This result suggests

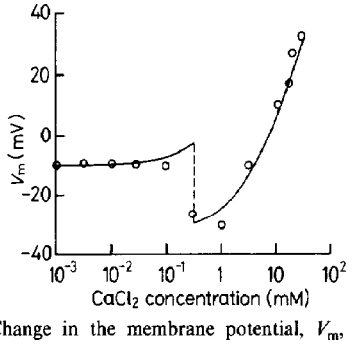

Fig. 3. Change in the membrane potential, V_m, caused by Ca^{2+}. Experimental situation is the same as in Fig. 2. (○) Experimental data, (—) theoretical curve of eq. (2) using parameter values listed in Table 1.

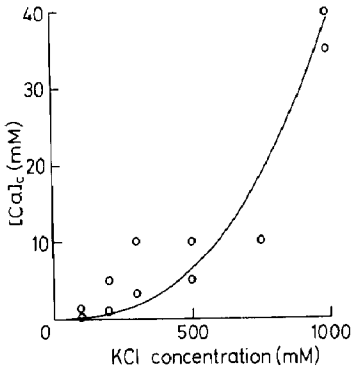

Fig. 4. Dependence of $[Ca]_c$ on K^+ concentration. The Na^+ concentration was kept at 100 m*M*. (○) Experimental data, (—) theoretical curve of eq. (5) with $\eta = 0.5$ using parameter values listed in Table 1.

that more Ca^{2+} ions are required for maintaining a high membrane resistance when more K^+ ions are included in the cell. This is a well-known antagonistic phenomenon observed also in other kinds of lipid phase transitions taking place in the presence of Ca^{2+} (or H^+) and K^+ (or Na^+) ions [15–17]. Binding of Ca^{2+} to DOPH can be inhibited by the coexisting monovalent cations.

3.3 Observation of the surface structure of membrane

The SEM photographs of the surface structure of the membrane are shown in Fig. 5. For the

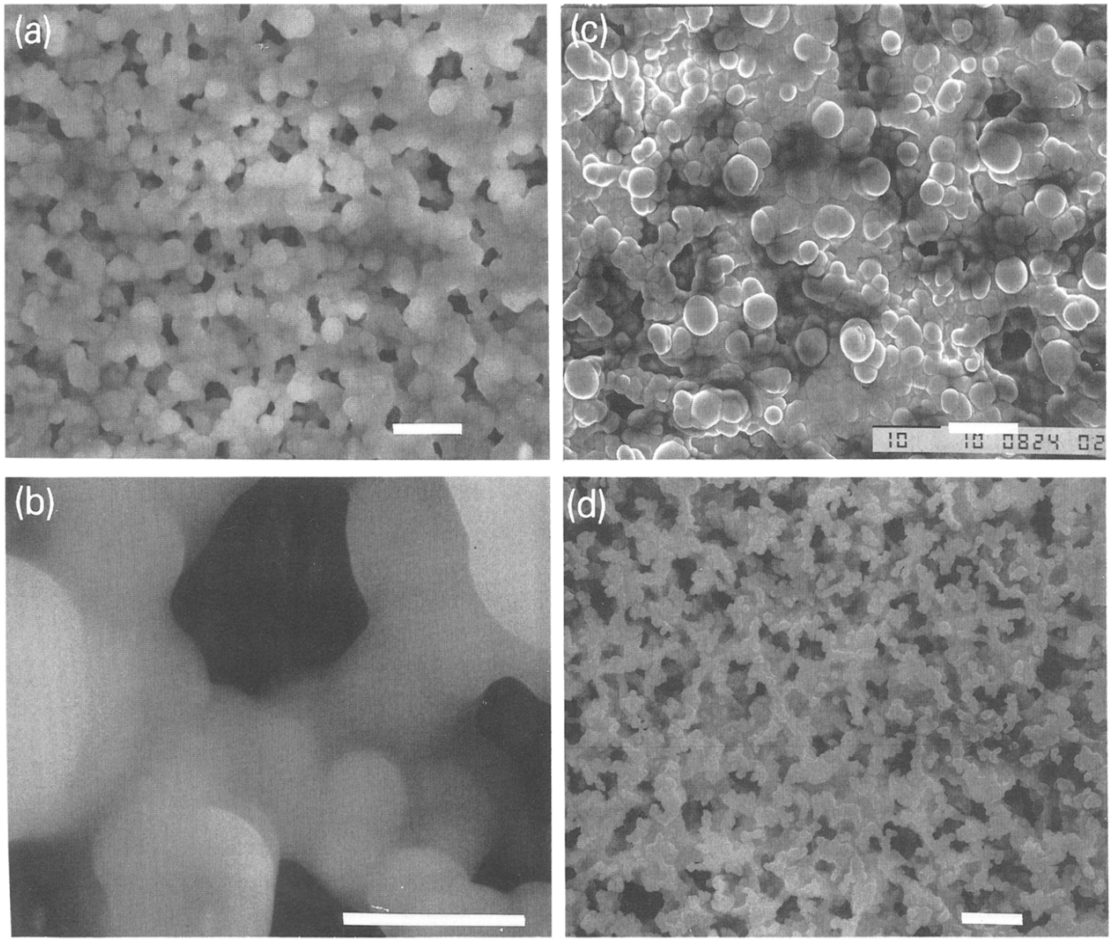

Fig. 5. SEM photographs of the surface structure of the membrane. (a) and (b) 100 m*M* NaCl; (c) 100 m*M* NaCl + 3 m*M* $CaCl_2$; (d) 100 m*M* NaCl + 3 m*M* $CaCl_2$ + 300 m*M* KCl. The horizontal bars imply 10 μm in length in (a), (c), (d) and 3 μm in (b).

DOPH membrane in 100 mM NaCl solution (Figs. 5a and b), the pores of about 5 μm in diameter can be seen as shaded domains. This observation agrees with the result in Fig. 2 that the membrane electrical resistance is low due to the formation of micelles and a bilayer structure, which is a compact state [7,8]. On the contrary, the oil droplets entirely covering the filter pores can be seen in Fig. 5c under the condition of 100 mM NaCl + 3 mM $CaCl_2$.

Figure 5d shows the photograph obtained for the DOPH membrane treated with a mixed solution of 100 mM NaCl, 3 mM $CaCl_2$ and 300 mM KCl. Many pores can be seen; this result supports the result in Fig. 4, where the membrane resistance is low under this condition of highly concentrated monovalent cations.

3.4 Self-oscillation of the membrane potential

The membrane exhibited a self-oscillation of the electrical potential with a period of ~1–10 s and an amplitude of ~50–100 mV, which continued stably for about 1 hour, when external forces such as pressure and electrical current were imposed under Na^+, Ca^{2+}/K^+ gradient. Figure 6a shows an example of self-oscillations with a period of approximately 3 s observed when a pressure difference, ΔP, of 20 cm H_2O (2 kPa) and a d.c. electrical current, I, of 0.56 μA were imposed on the membrane from the 100 mM KCl side to the 100 mM NaCl + 3 mM $CaCl_2$ side. The pulses of the oscillation were in a downward (or depolarized, excited) direction. The oscillations appeared usually beyond some value of electrical current, which was ~0.2–0.4 μA under 20 cm H_2O, different for each membrane.

In Fig. 6b, the dependence of the oscillation frequency on the imposed d.c. electrical current is shown with a curve designating a theoretical result, mentioned below. The frequency increases with the electrical current.

3.5 Change of the membrane resistance during oscillation

Figure 7 shows an example of oscillations when the a.c. current was superimposed on the membrane. When the potential stays at the higher resting level, the membrane resistance is estimated at 3.0 MΩ. At the lower excited (depolarized) level, its resistance decreases to 2.1 MΩ.

The resistance did not fall, however, down to a few kΩ, which is the value in the absence of Ca^{2+}, as seen in Fig. 2. This suggests that not all pores are open but only one certain pore or a certain domain of the membrane is open. This interpreta-

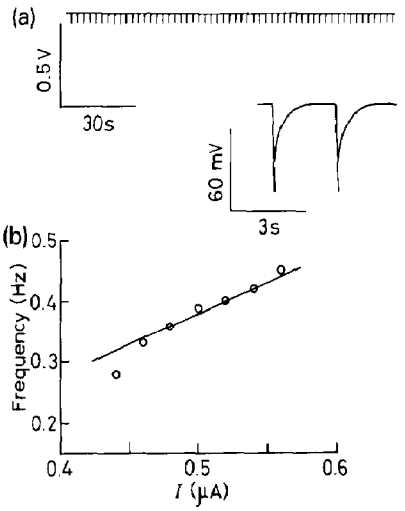

Fig. 6. Experimental data on self-oscillations. (a) A self-oscillation in the membrane placed between 100 mM KCl and 100 mM NaCl + 3 mM $CaCl_2$ under I = 0.56 μA and ΔP = 20 cm H_2O. (b) Dependence of the oscillation frequency on the imposed d.c. electical current. (○) Experimental data, (—) theoretical curve using parameter values listed in Table 1.

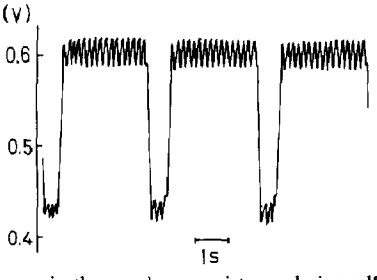

Fig. 7. Change in the membrane resistance during self-oscillation. The d.c. applied current was 0.2 μA with the sine wave of full amplitude 0.01 μA under 30 cm H_2O. The self-oscillation is given by the narrow downward deflections while the resistance measurement is superimposed on the oscillation by the small sine wave.

tion is consistent with our theory, which insists that only one single pore is responsible for the oscillation [4], and a recent experiment in which a fine minute pore was used for fixing DOPH molecules [18].

4. Theoretical model

4.1 Equivalent electrical-circuit model

The total system can be simulated by the equivalent electrical circuit shown in Fig. 8, where the DOPH membrane is represented by the circuit depicted on the left-hand side. This part is composed of a single pore with C, R and E participating in the oscillation, all the other pores being represented by C_0, R_0 and E_0.

The part showing the oscillation can be considered as one pore or several nearest pores behaving cooperatively. One reason is that we have often observed coexistent appearance of two kinds of oscillations with different amplitudes and periods [4]. Another reason is that an estimation of the electrical resistance of one open pore leads to a good match with observed data: Using the conductivity of 100 mM KCl (= 150 cm^2/Ω per equiv.), an open pore with the radius 2.5 μm and the length 100 μm gives the electrical resistance of about 3.4 MΩ. Since the membrane resistance R_m is several MΩ or more at high-resistance state, we get 5×10^6 MΩ as the electrical resistance of one "closed" pore because of 10^6 pores by adopting a value of, e.g. 5 MΩ for R_m. The electrical resistance of "one pore" can largely change from 5×10^6 MΩ to 3.4 MΩ. In this case, R_m decreases to $5 \times 3.4/(5 + 3.4) = 2.0$ MΩ when one pore opens. We can conclude that the membrane resistance R_m can change between 5 MΩ and 2 MΩ while one pore is closed and then opens. This result is consistent with the result shown in Fig. 7.

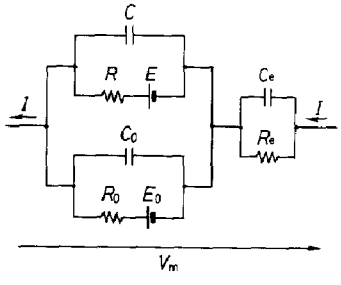

Fig. 8. Equivalent electrical-circuit model. The electrical quantities in the external aqueous solutions are denoted by C_e and R_e. The electrical characteristics of the membrane are expressed by the electrical circuit composed of the oscillating part (C, R, E) and non-oscillating part (C_0, R_0, E_0).

The values of C, R and E vary temporarily with the change in the conformational structure of DOPH assemblies. The change in the voltage across the condenser C is much faster than the rate of conformational change in DOPH [4]. Because of small values of C_e and R_e, we can safely approximate the membrane potential V_m by

$$V_m = \frac{R}{R_0 + R}(R_0 I - E_0) - \frac{R_0}{R_0 + R}E \qquad (1)$$

in the presence of applied electrical current I. Equation (1) can be derived because I is divided into two elements R_0 and R. Dependence of R on the conformational state of DOPH will be discussed in the next section. As for E_0, the sum of the diffusion potential within the membrane and the surface electrical potentials leads to (see Appendix A) [19,20]

$$E_0 = 59.2 \log \frac{P_K[K^+]_1}{P_{Na}[Na^+]_2 + P_{Ca}^{eff}[Ca^{2+}]_2}, \qquad (2a)$$

where E_0 is in mV at 25 °C, $[i]_j$ is the concentration of species i (K^+, Na^+ and Ca^{2+}) in the bulk phase j (= 1, 2) and P_{Ca}^{eff} is defined by

$$P_{Ca}^{eff} = P_{Ca} \exp(-eV_{S2}/k_B T). \qquad (2b)$$

The K^+ side is termed 'phase 1' and the $Na^+ + Ca^{2+}$ side is termed 'phase 2' for convenience. The absolute temperature, the elementary charge (> 0) and the Boltzmann constant are designated T, e and k_B, respectively. V_{S2} denotes the surface electrical potential at the $Na^+ + Ca^{2+}$ side, as detailed in Appendix A. P_K, P_{Na} and P_{Ca} are the coefficients of permeability of K^+, Na^+ and Ca^{2+} through the membrane, respectively.

The experimental situation in Fig. 3 leads to $R = R_0$ and $E = E_0$, because no external forces are applied on the membrane and the oscillation does not occur (i.e., the oscillating part R and E

disappears). The membrane potential V_m, therefore, is reduced to $-E_0$. The theoretical curve of eq. (2a) is shown in Fig. 3 by a solid line with $P_K/P_{Na} = 1.47$, $P_{Ca}^{eff}/P_{Na} = 105$ below 0.3 mM $CaCl_2$ and $P_K/P_{Na} = 3.55$, $P_{Ca}^{eff}/P_{Na} = 35.2$ above it. The ratio P_K/P_{Na} below 0.3 mM $CaCl_2$ was chosen as equal to the ratio of conductivity in the aqueous solution [21]. The reason of different values of the parameters between the low and the high Ca^{2+} concentrations is the transition from the low-resistance state to the high-resistance state (see Fig. 2). At present, however, it seems difficult to express the parameter values quantitatively by the state of DOPH assemblies.

4.2 Equations for phase transition of DOPH and ion concentration

Figure 9 illustrates the conformational states of DOPH in a pore under ΔP and I, where a DOPH molecule is illustrated as a small circle with two zigzag tails. K^+ and Ca^{2+} have an antagonistic effect with each other, as obtained in Fig. 4. At lower K^+ concentrations in the presence of Ca^{2+}, DOPH molecules make the hydrophobic phase but at much higher K^+ concentrations the hydrophilic phase. Binding of Ca^{2+} to DOPH molecule is affected greatly by the K^+ concentration. The length l of a 'phase-transition region', where repeated phase transitions could occur [3–5], is determined by diffusion of KCl which is enhanced by electrical current and pressure.

We simplify the situation by assuming homogeneities of both the state of DOPH assemblies and the ion concentration along the longitudinal axis of pore in the phase-transition region. Thus we consider the averaged quantities such as the fraction of micelles. Introduction of the phase-transition region simplifies the situation very much, because the longitudinal variation along the pore (i.e., perpendicular to the membrane surface) does not need to be considered [4,22,23]. The remaining region except for the phase-transition region is composed of multilayers due to the presence of over 100 mM KCl, and hence, this region may show the low electrical resistance and small potential difference.

Oil droplets are large aggregates composed of many loosely packed lipids in a random phase, which are shown schematically by the amorphous shapes occupied by dots in Fig. 9. Spherical micelles are, on the other hand, formed from approximately 100 lipids, and multilayers have

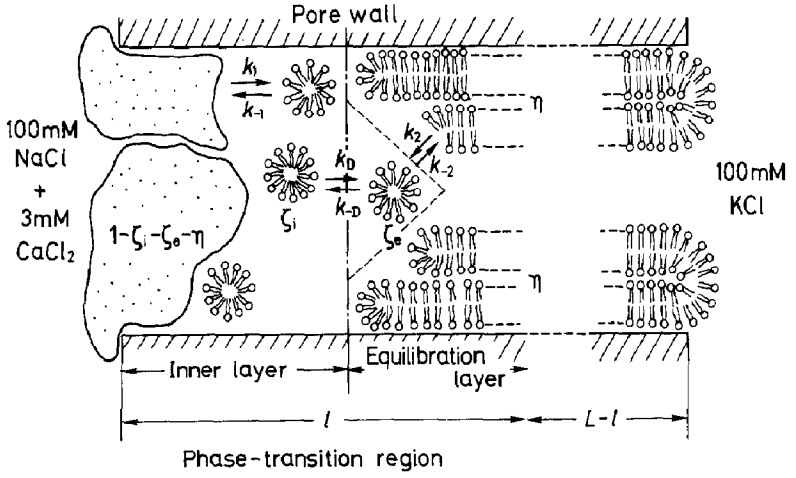

Fig. 9. Illustration of conformations of DOPH molecules within a pore. In the phase-transition region, the homogeneities are assumed for the ion concentrations and the conformational states of DOPH assemblies. The remaining region within the pore is not related to the oscillation, because the DOPH molecules tend to become multi-bilayers by high KCl concentrations. The length l of the phase-transition region is much shorter than the filter paper width L. The relevant rate constants are attached to reaction and conversion steps of DOPH assemblies.

planar lamellar structures with tight packing, while all polar head groups are in contact with the aqueous phase. A direct transformation, however, from oil droplets to multilayer may not occur so easily under usual conditions because of the large size of oil droplets. In the model, therefore, oil droplets are supposed to be transformed to many small micelles at the first stage of increasing K^+ concentration. Thereafter some of them diffuse into an equilibration layer, inside which they can make electrical and Van der Waals interactions with multilayer.

Here ζ_i, η and ζ_e are defined as the fraction of DOPH in micelles in inner bulk layer far from the pore wall, that in multilayers and that in micelles in equilibration layer, respectively. We designate ζ and n the total fraction of micelles ($=\zeta_i+\zeta_e$) and the monovalent-cation concentration ($=n_K+n_{Na}$), respectively, where n_K designates the average concentration of K^+ in the phase-transition region, n_{Na} being the Na^+ concentration.

Because the theoretical scheme is almost the same as that presented previously [3–5], the full description is made in Appendix B. The only difference is the explicit inclusion of the Ca^{2+} effect. After the parameter values are determined by explaining the static data in Figs. 2 and 4, self-oscillations are described using the equations for the phase transition of DOPH.

Equations (B5) and (B10) describe kinetics of phase transition of DOPH and K^+ concentration in the phase-transition region. We must connect ζ, η and n to the observed quantities.

5. Comparison with observed data

The membrane electrical resistance decreases as the multilayer is formed. It may be reasonable, therefore, to regard R in Fig. 8 as a decreasing function of the fraction of multilayer η:

$$R = r_1 - r_2(\eta - \eta_{min})^{\alpha}, \tag{3a}$$

with r_1, r_2, η_{min} and α denoting the numerical parameters. Since V_m directly reflects R, selection of the values of η_{min} and α is important to express the wave form of membrane potential. Equation (3a) concerns one pore participating the oscillation, and hence treats a small variation. Whereas the lengthy expression for R can be obtained using a constant field theory [19,20], eq. (3a) is sufficient for describing the behaviors of the DOPH membrane. The membrane resistance is given by

$$R_m = \frac{RR_0}{R+R_0}. \tag{3b}$$

Now let us discuss the static property in Fig. 2. In this case, a large variation of membrane electrical resistance occurs due to the contribution from many pores. This can be acknowledged as follows: An open pore has an electrical resistance of about 3 MΩ while the membrane resistance R_m takes a value of about 10 MΩ in its high-resistance state (i.e., when all pores are closed). If one pore is open, then R_m becomes $10\times 3/(10+3)=2.3$ MΩ. If 10 pores are open, R_m becomes $10\times 0.3/(10+0.3)=291$ kΩ; R_m decreases to $10\times 0.03/(10+0.03)=30$ kΩ for 100 open pores. This result implies that only if $100/10^6=0.01\%$ of all pores are open, will R_m decrease drastically (by three orders) from 10 MΩ to 30 kΩ. Because we try to express R_m, we must consider the change in the number of open pores quantitatively in addition to consideration of R in one pore by eq. (3a). It requires another stochastic approach. In the experimental situation of Fig. 2, therefore, we had better reconsider that η reflects the average behavior of all pores by adopting directly the sharp decreasing function of η as R_m

$$R_m = \frac{R_l R_h}{(1-\hat{\eta})R_l + \hat{\eta}R_h}, \tag{4a}$$

where $\hat{\eta}$ is given by

$$\hat{\eta} = \eta u(\eta - \hat{\eta}_c), \tag{4b}$$

with $u(x)$ being a step function:

$$u(x) = \begin{cases} 0 & ; x \le 0, \\ 1 & ; x > 0. \end{cases} \tag{4c}$$

In the above expressions, R_l and R_h provide the measures of membrane resistance at lower and higher Ca^{2+} concentrations, respectively. The step

function with one parameter $\hat{\eta}_c$ is introduced to describe the sharp variation of R_m.

The results in Figs. 2 and 4 can be explained quantitatively using the above expressions: The static solution of η is obtained from eqs. (B5) as a function of ion concentrations $n(=[K^+]_1 + [Na^+]_2)$ and n_2 $(=[Ca^{2+}]_2)$:

$$\eta = \left[1 + \frac{\upsilon}{K_{20}} \frac{\sqrt{n_2}}{n} \left(1 + \frac{k_{-1}}{k_1 n}\right)\right]^{-1}, \qquad (5)$$

where υ $(\gg 1)$ and K_{20} are introduced by eqs. (B3) and (B7), respectively. Since eq. (5) contains $\sqrt{n_2}/n$, K^+ and Na^+ compete with Ca^{2+}. Substitution of eq. (5) into eq. (4a) gives a theoretical curve shown in Fig. 2, which explains the observed data well with the parameters in Table 1.

The relation between $n_2 = [Ca]_c$ and $n = [K^+]_1 + [Na^+]_2$ is given by the curve of eq. (5) by putting $\eta = 0.5$, because the membrane electrical resistance must change around $\eta = 0.5$. Agreement between the experimental data and the theoretical result in very good, as seen in Fig. 4.

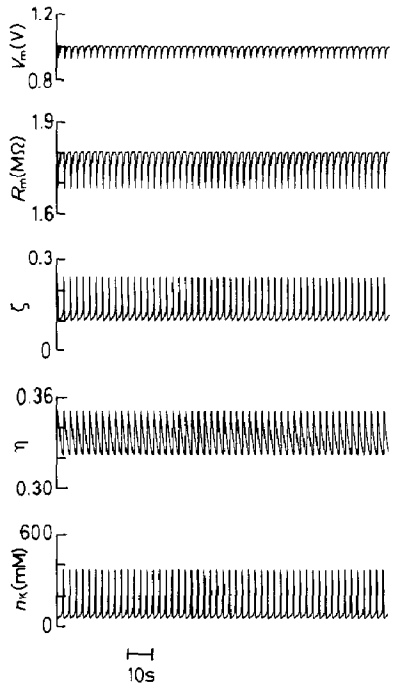

Fig. 10. Theoretical results of a self-oscillation under 100 mM + 3 mM $CaCl_2$/100 mM KCl with the electrical current, 0.56 μA. The numerical parameters are given in Table 1. The NaCl and $CaCl_2$ concentrations were fixed at $n_{Na} = 100$ mM and $n_2 = 3$ mM.

Table 1

Values of numerical parameters. The rate constants such as k_1^* in eqs. (B8) for kinetics of DOPH assemblies were chosen almost equal to the previously adopted values [4,5]. The diffusion constant estimated from D^* for K^+ amounts to approximately 10^{-6} cm^2/s, which is reasonable within pores containing DOPH because of the smaller values than approx. 10^{-5} cm^2/s in water. Parameters for the electrical resistances such as r_1 were chosen so as to express the observed values. The value of υ in parentheses was chosen for good explanation of Fig. 4. The parentheses values for P_K/P_{Na} and P_{Ca}^{eff}/P_{Na} indicate the values above 0.3 mM $CaCl_2$, as detailed in text

Parameter	Value	Parameter	Value
k_1^*	2.44×10^{-3} s^{-1} mM^{-1}	r_1	2.2 MΩ
k_{-1}^*	2.0 s^{-1}	r_2	6.0 GΩ
K_{20}	1.0 m$M^{-1/2}$	η_{min}	0.32
k_D^*	1.5×10^{-5} s^{-1}	α	3.0
D^*	9.5×10^{-3} s^{-1}	R_1	3.0 kΩ
υ	45.0 (101)	R_h	7.0 MΩ
A	0.01	$\hat{\eta}_c$	0.6
B	0.5	R_0	10 MΩ
N	1.0×10^3 mM	P_K/P_{Na}	1.47 (3.55)
ζ_c, η_c	0.2	P_{Ca}^{eff}/P_{Na}	105 (35.2)
γ	3.5	I_0	2.37 nA
λ	3.0	I_c	0.064 μA

The coupled eqs. (B5) and (B10) concerning ζ, η and n_K were solved numerically for explanation of oscillations, and the results were substituted to eq. (1) for V_m. Because the electromotive force E is as small as E_0 compared with the change in V_m occurring in Fig. 6a, a difference between E and E_0 can be neglected safely in oscillations; E and E_0 were put to 10 mV from Fig. 3. The electrical oscillations can be analyzed using eqs. (B5) and (B10) with the parameter values, which were already determined to explain quantitatively the steady-state curves in Figs. 2 and 3.

Figure 10 shows the simulation results of V_m of eq. (1), R_m of eq. (3b), ζ, η and n_K. The numerical parameters are listed in Table 1. The wave form of relaxation-oscillation type and the frequency of V_m reproduce well the measured electrical voltage showing a sharp spike in Fig. 6a.

The membrane resistance R_m decreases when V_m is depolarized, in agreement with the observed data in Fig. 7. The phase transition of DOPH is repeated synchronous with accumulation and release of K^+ ions.

The dependence of the oscillation frequency on the imposed d.c. electrical current is compared with the experimental data in Fig. 6b. The agreement may be fairly good. The increasing frequency is due to both the decreasing DOPH molecules concerned with oscillations and the accelerated K^+ diffusion, which are expressed by eqs. (B8) and (B12) through eq. (B9), respectively.

6. Discussion

The membrane resistance of the DOPH membrane was increased drastically by addition of Ca^{2+} under the 100 mM NaCl/100 mM KCl gradient. This phenomenon was explained quantitatively by binding of Ca^{2+} to DOPH molecules. Calcium ion bound to DOPH was detached by application of highly concentrated monovalent cations.

The present theory takes into account this antagonistic effect, as revealed by Fig. 4, and can explain the oscillation based on this fact. While the phase transition previously studied [1–5] is caused by the electrostatic screening due to K^+ or Na^+ cations leading to the low-resistance state, the transition studied here is concerned with the Ca^{2+} binding to DOPH, which leads to the high-resistance state. This situation was visualized by the surface structure of the membrane in Fig. 5; i.e., we can understand intuitively that the low-resistance state is de to opening of pores.

The values of P_K/P_{Na} and P_{Ca}^{eff}/P_{Na} above 0.3 mM $CaCl_2$ were chosen to be larger and smaller than those below it, respectively, in Fig. 3. The reason of larger values of P_K/P_{Na} above 0.3 mM $CaCl_2$ is that the relative permeability to K^+ is increased due to the increase in the membrane resistance, as in Fig. 2. In fact, the membrane potential showed a large negative value, which implies the higher K^+ permeability, in the high-resistance state [6]. It is noticeable that the permeability to K^+ was increased by tiny amounts of

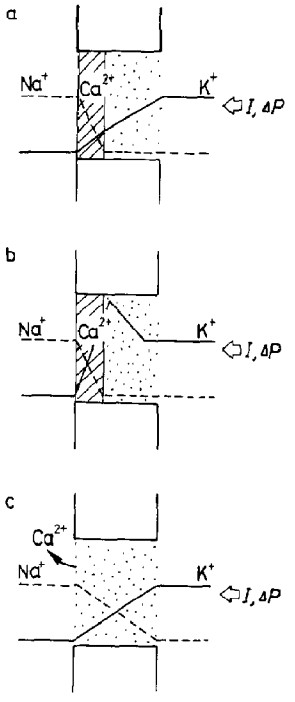

Fig. 11. Illustration of states of DOPH and ion concentration within a pore during self-oscillation. Dots denote DOPH with the low resistance, the shaded part implying high-resistance DOPH. The solid and the broken lines show the K^+ and the Na^+ concentrations, respectively. External forces such as electrical current and pressure are imposed from the KCl side to the NaCl + $CaCl_2$ side.

Ca^{2+}. The smaller value of P_{Ca}^{eff}/P_{Na} above 0.3 mM $CaCl_2$, on the other hand, is due to the decrease in the magnitude of the surface potential V_{S2} in eq. (2b). Adsorption of Ca^{2+} on the DOPH membrane causes the decrease in the surface charge density, which leads to the decrease in $|V_{S2}|$, as is well known [15–17].

Figure 11 illustrates the mechanism of the self-sustained oscillation of the membrane potential based on Fig. 10. The external forces are imposed on the membrane from the K^+ side to the $Na^+ + Ca^{2+}$ side. When the membrane is placed between 3 mM $CaCl_2$ + 100 mM NaCl and 100 mM KCl, the membrane resistance indicates the high value due to the binding of Ca^{2+} to DOPH, which may occur near the $Na^+ + Ca^{2+}$ side (Fig. 11a). The numerical simulation in Fig. 10 shows that n_K is low while R_m is high. In Fig. 11, the K^+ con-

centration is illustrated by a solid line, while that of Na^+ by a broken line. The shaded part implies the lipids which maintain the high resistance, the dotted part showing the low resistance. Potassium ions penetrate into the membrane driven by the electrical current and pressure difference. As a result, K^+ accumulates near the $Na^+ + Ca^{2+}$ side composed of lipids bound by Ca^{2+} (Fig. 11b).

When the K^+ concentration becomes higher than some critical concentration, shown in Fig. 4, Ca^{2+} bound to DOPH can be replaced by K^+. Thus, Ca^{2+} leaves from the DOPH membrane and the membrane resistance becomes lower (Fig. 11c). In the numerical simulation of Fig. 10, R_m drastically decreases with the abrupt increase in n_K. The threshold concentration of K^+ which causes release of Ca^{2+} is about 200 mM (Fig. 4). This value is easily attainable due to the external forces of electrical current and pressure difference. Due to the change to the low-resistance state, K^+ which has accumulated within the pore is released; then the K^+ concentration within the pore becomes low. The membrane resistance, therefore, becomes high again because of the binding of Ca^{2+} to DOPH. This is the first step shown in Fig. 11a. Therefore the repetition of this process gives rise to the electrical oscillation through the change in electrical resistance.

Previous studies show [24,25] that this lipid membrane can respond to various taste substances (flavours). Such functions of the biological membrane as excitability and taste perception will be realized by using only artificial lipid membranes. The DOPH-adsorbed membrane, however, lacks quantitative reproducibility; e.g., the oscillatory frequency differed from each sample and the duration of the oscillation diverged from a few minutes to a few hours. Development of artificial nerve cells, which can be used as neuro-computer elements, may need new artificial lipids and new fixation materials.

Recent study has shown that a thin film composed of cationic lipids and membranes comprising DOPH or other lipid species respond to flavours in different fashions [23,26]. From our experience we know that the electrical oscillation can easily be triggered when oleyl alcohol is mixed with DOPH and the blend is allowed to become oxidized to some extent. The surface structures were found to be also different in these mixed lipid membranes. The mixing and oxidizing procedures, therefore, seem to be important for useful membrane preparation. A set of different kinds of lipid membranes will be effective for artificial nerve cells, which respond to flavours or work as information-processing elements in neuro-computer devices. Electrical behaviors in coupled lipid-membrane elements might be very interesting.

Appendix A

We introduce V_{S1} and V_{S2} defined by the surface potentials formed near the boundary surfaces of the membrane at phase 1 containing 100 mM KCl and phase 2 containing 100 mM NaCl with an arbitrary concentration of $CaCl_2$, respectively. The surface potential is either of the Donnan or Gouy–Chapman double-layer type depending on the charged state near the surface of the membrane [27]. The membrane potential V_m^0 measured taking phase 2 as the origin is given by summation of the diffusion potential within the membrane V_d and the surface-potential difference $V_{S2} - V_{S1}$:

$$V_m^0 = V_d + V_{S2} - V_{S1}. \tag{A1}$$

The steady-state diffusion potential V_d (in mV) is calculated using the constant field theory [19]:

$$V_d = -59.2 \log \frac{P_K[K^+]_{S1} + P_{Cl}[Cl^-]_{S2}}{P_{Na}[Na^+]_{S2} + P_{Cl}[Cl^-]_{S1} + P_{Ca}[Ca^{2+}]_{S2}} \tag{A2}$$

at 25 °C. The permeabilities are denoted by P_i for $i = K^+$, Cl^-, Na^+ and Ca^{2+}. Whereas the permeability to Ca^{2+} is modified by a coefficient, $4/[1 + \exp(eV_d/k_BT)]$, the value of P_{Ca} does not change so much because the membrane potential (and diffusion potential) is small, as seen in Fig. 3. The surface ion concentrations $[i]_{Sj}$ are defined by

$$[i]_{Sj} = [i]_j \exp(-z_i eV_{Sj}/k_BT) \qquad \text{for } j = 1, 2, \tag{A3}$$

where $[i]_j$ and z_i are the concentration of the bulk

phase j experimentally controlled and the valence of species i, respectively.

The DOPH membrane is charged so negatively that under a KCl concentration gradient it has a negative membrane potential on the side of the higher KCl concentration. This membrane potential shows a Nernst-type variation with KCl concentration [2,4]. Therefore P_{Cl} can be safely put to zero. Because the electromotive force $-E_0$ in Fig. 8 produced by the pore without contribution to oscillations does not change temporarily, it can be regarded as equal to V_m^0. Thus E_0 is given by eq. (2).

It is difficult to estimate the relative magnitudes of V_d and $V_{S2} - V_{S1}$, as is the case in usual membrane systems too. In the DOPH system, however, we can consider that $V_{S2} - V_{S1}$ largely contributes to V_m because effects of chemical substances on the membrane appeared fast, i.e. within a few minutes [24,25]. If the diffusion potential inside the membrane would be effective, the response might have been slower.

Appendix B

We describe the behavior of DOPH in the phase-transition region. Here ζ_i, η and ζ_e are defined as the fraction of DOPH in micelles in inner bulk layer far from the pore wall, that in multilayers and that in micelles in equilibration layer, respectively. While the symbols used here are different from those used in previous papers [3–5], micelles are now unified to ζ, and multilayers are denoted by η only for simplicity. The fraction of DOPH in oil droplets is $1 - \zeta_i - \zeta_e - \eta$. Kinetic equations for DOPH may have the same form as published previously [3–5]:

$$\frac{d\zeta_i}{dt} = k_1(1 - \zeta_i - \zeta_e - \eta)n - k_{-1}\zeta_i + k_{-D}\zeta_e - k_D\zeta_i, \tag{B1a}$$

$$\frac{d\zeta_e}{dt} = -k_{-D}\zeta_e + k_D\zeta_i + k_{-2}\eta - k_2\zeta_e, \tag{B1b}$$

$$\frac{d\eta}{dt} = -k_{-2}\eta + k_2\zeta_e, \tag{B1c}$$

where the coefficients k_1, k_{-1}, k_2, k_{-2}, k_D and k_{-D} designate the relevant rate constants, and n is the monovalent-cation concentration:

$$n = n_K + n_{Na}, \tag{B2}$$

where n_K and n_{Na} designate the average concentrations of K^+ and Na^+ in the phase-transition region, respectively.

The rate constants k_D and k_{-D} reflect a relation between a diffusion constant and a free volume:

$$k_D = k_{-D}/v, \tag{B3}$$

where v designates the volume ratio of the equilibration layer to the inner one. The free volume, within which DOPH can move freely, is increased with the developing multilayer phase.

If we consider an electrochemical free energy of the system comprising the charged multilayer and aqueous solution, where monovalent ions form an electrical double layer near the lipid bilayer and Ca^{2+} is bound to two lipid molecules, then we get [5,17]

$$k_{-2} = k_{-2}^0\sqrt{n_2}/n, \tag{B4}$$

where n_2 denotes the Ca^{2+} concentration and k_{-2}^0 is a constant. The phase transition of DOPH is affected by Ca^{2+} through k_{-2}. Equation (B4) expresses the antagonistic effect between monovalent and divalent cations.

Because k_2 and k_{-2} are much larger than other rate constants, the reaction given by eq. (B1c) is much faster than the reactions of eqs. (B1a) and (B1b). We can therefore safely approximate $d\eta/dt = 0$ in eq. (B1c). As a result, the temporal change in η is attributed to those in ζ_i and ζ_e described by eqs. (B1a) and (B1b). Adding eq. (B1a) to eq. (B1b), we obtain

$$\frac{d\zeta}{dt} = k_1(1 - \zeta - \eta)n - k_{-1}\left(\zeta - \eta\sqrt{n_2}/K_{20}n\right), \tag{B5a}$$

where ζ is the total fraction of micelles defined by

$$\zeta = \zeta_i + \zeta_e, \tag{B6}$$

and $K_{20}n/\sqrt{n_2}$ refers to the rate constant for the transformation between micelles and multilayer:

$$K_{20}n/\sqrt{n_2} = k_2/k_{-2} = k_2n/\sqrt{n_2}k_{-2}^0. \tag{B7}$$

Furthermore, eq. (B1b) can be approximated by

$$\frac{d\eta}{dt} = k_D\left(K_{20} n\zeta/\sqrt{n_2} - v\eta\right), \qquad \text{(B5b)}$$

where $(v+1)$ was replaced by v ($\gg 1$). Since eq. (B5b) describes a slow change in η resulting from eq. (B1b), it does not contradict with the approximation $d\eta/dt = 0$ of eq. (B1c), which eliminates the fast component of change in η.

Because eqs. (B1) or (B5) represent overall sequential reactions of DOPH assemblies inside the phase-transition region of the length l, the rate constants should depend on the number of DOPH molecules contributing to self-oscillations in this region. The values of such rate constants may, therefore, increase with the decrease in the number of concerning molecules. The number of molecules may decrease while the length l does: the rate constants are considered as decreasing functions of l. Thus we assume the following simple relation between them:

$$k_1 = k_1^*/(l/L), \qquad k_{-1} = k_{-1}^*/(l/L)$$

$$\text{and } k_D = k_D^*/(l/L), \qquad \text{(B8)}$$

where L is the filter width and the quantities with an asterisk are constant.

Equations (B5) with the rate constants of eqs. (B3), (B7) and (B8) are the basic equations to describe kinetics of phase transition of DOPH in the presence of electrical current I and pressure. Dependence of l/L on I can be assumed as a decreasing form similar to a previous one [3–5]:

$$l/L = l_0/(I - I_c), \qquad \text{(B9)}$$

with l_0 and I_c denoting numerical parameters. Equation (B9) is applicable to $I > I_c$ because I_c is smaller than the value of I (usually larger than 0.2 μA) to cause the oscillation.

Next, let us mention a kinetic equation for the monovalent-cation concentration n, which is the average quantity in the phase-transition region. The width of this region is very narrow [4,5,22]. We can, therefore, assume that the Na^+ concentration n_{Na} in this region is close to that of the bulk solution, i.e., $n_{Na} = 100$ mM. The K^+ concentration, on the other hand, depends on diffusion from the KCl side to the $NaCl + CaCl_2$ side:

$$\frac{dn_K}{dt} = D(\hat{n}_K + n_K), \qquad \text{(B10)}$$

where D is the diffusion constant of K^+ and $\hat{n}_K$ is the stationary concentration given by [4,5,18]

$$\hat{n}_K = \frac{N\left[A + (\zeta/\zeta_c)^\gamma\right]\left[1 + B(\eta/\eta_c)^\lambda\right]}{\left[1 + (\zeta/\zeta_c)^\gamma\right]\left[1 + (\eta/\eta_c)^\lambda\right]}, \qquad \text{(B11)}$$

where N, A (< 1) and B (< 1) are the numerical parameters for expressing the magnitude of n_K. The maximum of eq. (B11) is N, and may reach about 1 M due to accumulation forced by electrical current and pressure. While the minimum is NAB, the K^+ concentration may decrease to 1 mM or so. The functional form with the numerical constants γ, λ, ζ_c and η_c is adopted so as to express the property that the multilayer phase releases cations while the spherical-micelle phase accumulates cations.

The diffusion constant D depends on the square of the length of the concerning region in the usual way:

$$D = D^*/(l/L)^2, \qquad \text{(B12)}$$

with D^* denoting the numerical constant dependent on the amount DOPH adsorbed.

References

1 N. Kamo, T. Yoshioka, M. Yoshida and T. Sugita, J. Membrane Biol. 12 (1973) 193.
2 Y. Kobatake, Adv. Chem. Phys. 29 (1975) 319.
3 K. Toko, K. Ryu, S. Ezaki and K. Yamafuji, J. Phys. Soc. Jpn. 51 (1982) 3398.
4 K. Toko, M. Tsukiji, S. Ezaki and K. Yamafuji, Biophys. Chem. 20 (1984) 39.
5 K. Toko, M. Tsukiji, S. Iiyama and K. Yamafuji, Biophys. Chem. 23 (1986) 201.
6 S. Iiyama, K. Toko and K. Yamafuji, Biophys. Chem. 28 (1987) 129.
7 Y. Kobatake, A. Irimajiri and N. Matsumoto, Biophys. J. 10 (1970) 728.
8 K. Toko, J. Nitta and K. Yamafuji, J. Phys. Soc. Jpn. 50 (1981) 1343.
9 I. Tasaki, K. Kusano and P.M. Byrne, Biophys. J. 55 (1989) 1033.

10 D.E. Rumelhart, J.L. McClelland and the PDP Research Group, Parallel distributed processing (The MIT Press, Cambridge, MA, 1986).
11 J.Arisawa and T. Furukawa, Trans. Inst. Electron. Commun. Eng. J62-C (1979) 645.
12 K. Misawa and J. Arisawa, Maku (Membrane) 12 (1987) 42.
13 J. Arisawa and K. Misawa, J. Membrane Sci. 35 (1988) 231.
14 K. Yoshikawa, K. Sakabe, Y. Matsumoto and T. Ota, Biophys. Chem. 21 (1985) 33.
15 H. Trauble and H. Eibl, Proc. Natl. Acad. Sci. USA. 71 (1974) 214.
16 H. Trauble, M. Teubner, P. Woolley and H. Eibl, Biophys. Chem. 4 (1976) 319.
17 K. Toko and K. Yamafuji, Biophys. Chem. 14 (1981) 11.
18 K. Toko, S. Iiyama, K. Hayashi, N. Ozaki and K. Yamafuji, J. Phys. Soc. Jpn. 57 (1988) 2864.
19 A.B. Hope, Ion transport and membranes—A biophysical outline, chap. 1 (Butterworth, London, 1971).
20 S. Iiyama, Y. Suezaki, K. Toko, T. Murata, I. Ueda, H. Kamaya and K. Yamafuji, Biophys. Chem. 36 (1990) 141.
21 R.A. Robinson and R.H. Stokes, Electrolyte solutions (Butterworth, London, 1955).
22 K. Toko, T. Yoshida, K. Yamafuji, S. Iiyama, N. Nakashima and T. Kunitake, Proc. 6th Sensor Symp., ed. K. Takahashi (Institute of Electrical Engineers of Japan, 1986) p. 225.
23 K. Hayashi, K. Yamafuji, K. Toko, N. Ozaki, T. Yoshida, S. Iiyama and N. Nakashima, Sensors and Actuators 16 (1989) 25.
24 S. Iiyama, K. Toko and K. Yamafuji, Agric. Biol. Chem. 50 (1986) 2709.
25 K. Toko, K. Hayashi, S. Iiyama and K. Yamafuji, Dig. Tech. Papers of Transducers '87, in: Proc. 4th Int. Conf. Solid-State Sensors and Actuators, Maku (Membrane) 14 (1987) 793.
26 M. Saito, T. Koyano, Y. Miyamoto, K. Kaifu, M. Kato and K. Kawamura, Abs. 2nd Int. Symp. Bioelectronic & Mol. Electro. Devices (1988) 123.
27 H. Ohshima and T. Kondo, Biophys. Chem. 29 (1988) 277.